Journal of Alloys and Compounds 509 (2011) 5877–5881

Contents lists available at ScienceDirect

Journal of Alloys and Compounds

journal homepage: www.elsevier.com/locate/jallcom

A-site-disorder-dependent magnetocaloric properties in the mono-valent-metal doped $La_{0.7}Ca_{0.3}MnO_3$ manganites

Changyi Hao[a], Bangchuan Zhao[b,*], Yanan Huang[b], Guangli Kuang[a], Yuping Sun[a,b]

[a] High Magnetic Field Laboratory, Chinese Academy of Sciences, Hefei 230031, People's Republic of China
[b] Key Laboratory of Materials Physics, Institute of Solid State Physics, Chinese Academy of Sciences, Hefei 230031, People's Republic of China

ARTICLE INFO

Article history:
Received 15 December 2010
Received in revised form 24 February 2011
Accepted 27 February 2011
Available online 5 March 2011

PACS:
75.30.Sg
61.72.Ww

Keyword:
Magnetocaloric
Mono-valent-metal
Disorder

ABSTRACT

The influence of mono-valence-metal (Li, Na, and K) doping effect on the structural, resistivity, magnetic and magnetocaloric properties of $La_{0.7}Ca_{0.3}MnO_3$ polycrystalline samples is studied for a fixed (5% at Ca site) dopant concentration. All the samples crystallize in orthorhombic structure and the lattice parameters increase continuously as the dopant atoms changes from Li to Na and then K. Paramagnetic–ferromagnetic phase transition at T_C and insulator–metal phase transition at T_p are observed for all studied samples. The transition temperature decreases as Ca atoms is replaced by Li, while the transition temperature shifts to higher values as Ca is substituted by Na or K. In addition, the maximum magnetic entropy change of the K-doped sample is much smaller than that of the free- and Na-doped samples. The results are discussed according to the change of A-site-disorder effect caused by the systematic variations of A-site average ionic radius $\langle r_A \rangle$ and A-site-cation mismatch σ^2.

1. Introduction

Recently, hole-doped colossal magnetoresistance (CMR) manganites with a general formula $R_{1-x}A_xMnO_3$ (R = rare-earth ions, A = divalent ions) have been a subject of intensive research in view of their special electronic and magnetic properties as well as the potential applications [1]. It is commonly believed now that the double-exchange (DE) interaction plays an essential role to realize the nature of the CMR effect [2]. In these hole-doped manganites compounds, the physical properties are found to be controlled by two key factors: the hole-doping level x (Mn^{3+}/Mn^{4+} ratio) and the average ionic radius of the A-site elements $\langle r_A \rangle$ [3–8]. In order to stabilize the low temperature DE interaction and then the ferromagnetic (FM) metallic phase, hole doping level x in the range of 0.2–0.5 is needed and the optimum value of x is 0.33. The principle effect of decreasing $\langle r_A \rangle$ in hole-doped manganites is to reduce the Mn–O–Mn bond angle and then reducing the matrix element b that described electron hopping between adjacent Mn ions. This evidences a very strong coupling of electronic motion to lattice effects in these hole-doped manganites. The further lattice effect can be described by the A-site-cation mismatch giving by $\sigma^2 = \sum y_i r_i^2 - \langle r_A \rangle^2$ (y_i: fractional occupancy), which has also been shown to influence the physical properties of $R_{1-x}A_xMnO_3$ compounds strongly [9,10].

Except for CMR effect, another very important property, large magnetocaloric effect (MCE) under a moderate applied magnetic field, have been found for perovskite manganites in recent years [11,12], revealing that these manganite materials are possible candidate for magnetic refrigeration applications [13]. MCE is an intrinsic property of magnetic materials and induced by the strong coupling of magnetic sublattices with an applied magnetic field. The applied magnetic field in the material can induce a spin reorientation and then the decrease of spin entropy. When the process is adiabatic, the lattice entropy increases and temperature of the system increases. Inversely, when a magnetic field is removed from the material the spins tend to become random, which increases the entropy and causes the material to cool off. In general, the large magnetic entropy change in perovskite manganites originates mainly from the variation of the DE interaction between Mn^{3+} and Mn^{4+} ions arising from the change of Mn^{3+}/Mn^{4+} ratio. Therefore, many researchers tried to tune the magnetic entropy change in manganite materials by controlling the relative ratio Mn^{3+}/Mn^{4+} through the element substitution by the divalent or mono-valent ions, especially the mono-valent ions [9,14–18]. In order to further understand the nature of the mono-valent element doping effect in these systems, we present a systematic investigation of structural, magnetic, transport and MCE properties of Li-, Na-, K- and free-doped $La_{0.7}Ca_{0.3}MnO_3$ system at a fixed doping level $x = 0.05$. Hereafter, the four studied samples denote as $La_{0.7}Ca_{0.25}A_{0.05}MnO_3$

* Corresponding author. Tel.: +86 551 559 1439; fax: +86 551 559 1434.
E-mail address: bchzhao@issp.ac.cn (B.C. Zhao).

0925-8388/$ – see front matter © 2011 Elsevier B.V. All rights reserved.
doi:10.1016/j.jallcom.2011.02.162

(A = Li, Na, K and Ca). The obtained results show that the physical properties of the studied samples are sensitive to the average A-site ionic radius $\langle r_A \rangle$ and the A-site-cation mismatch σ^2.

2. Experimental

The polycrystalline manganite materials with compositional formula $La_{0.7}Ca_{0.25}A_{0.05}MnO_3$ (A = Li, Na, K and Ca) were prepared by sol–gel method using metal oxides and carbonates as starting materials. Stoichiometric amounts of high-purity La_2O_3, $CaCO_3$ and Li_2CO_3 (or Na_2CO_3, K_2CO_3) powders were dissolved in diluted nitric acid in which an excess of citric acid was added, followed by the addition of stoichiometric amounts of $Mn(NO_3)_2$ 50% solution with continuous stirring for about 12 h. After all reactants had been completely dissolved, the solution was heated on a hot plate resulting in the formation of a gel. The gel was dried at 350 °C, and then preheated to 550 °C to remove the remaining organic and decompose the nitrates of the gel. The obtained powders were ground, palletized, and sintered at 1400 °C for 10 h, and finally, the furnace was slowly cooled down to the room temperature.

The structure and phase purity of the studied samples were examined by the powder X-ray diffraction (XRD) using a Philips X'pert PRO X-ray diffractometer with Cu Kα radiation (λ = 1.5406 Å) at room-temperature. The composition of the result compound is determined by an energy dispersive spectroscopy (EDS) attached to the FEI thermal field emission scanning electron microscope equipment. The electrical transport properties were measured using the standard four-probe method in a commercial physical property measurement system (PPMS). The magnetic measurements were performed with a quantum design magnetic property measurement system (MPMS) in the temperature range of 5–350 K and field range from −4.52 T to 4.52 T.

3. Results and discussion

For structural determination, room temperature X-ray powder diffraction patterns for $La_{0.7}Ca_{0.25}A_{0.05}MnO_3$ (A = Li, Na, K and Ca) samples were performed and the results are shown in Fig. 1. The result shows that all the studied samples are single phase and characterize in the orthorhombic structure with *Pnma* space group. The structural parameters for all samples are refined by the standard Rietveld technique and a typical fitting result for the K-doped sample is shown in Fig. 2 as an example. The obtained structural parameters are listed in Table 1. From the table, we can see that the lattice parameters (*a*, *b*, and *c*) and the unit cell volume *V* of the Li-, Na-, and K-doped samples increase monotonously with increasing the average A-site cation radius $\langle r_A \rangle$. In order to clarify, the values of $\langle r_A \rangle$ together with A-site-cation mismatch of the studied samples are also listed in Table 1. In the table, standard ionic radii using the coordination number eight with values 1.16, 1.12, 0.92, 1.18 and 1.51 Å for La^{3+}, Ca^{2+}, Li^+, Na^+ and K^+, respectively, are used to calculate $\langle r_A \rangle$ and σ^2 [14,19]. It should be noted that the unit cell volume of all mono-metal-doped-samples is smaller than that of the free-doped sample $La_{0.7}Ca_{0.3}MnO_3$. The smaller unit cell volume of the mono-metal-doped samples can be explained by the increased Mn^{4+} content in Mn^{4+}/Mn^{3+} ratio and by the increase of the disorder of A-site [16]. The average grain size of the studied samples is estimated through the classical Scherrer formula [20] $D_{hkl} = k\lambda/\beta\cos\theta$, where D_{hkl} is the grain size derived from the (1 2 1), (2 0 2), and (1 2 3) peaks of the XRD patterns, *k* is the shape factor constant (∼0.9), θ is the angle of the diffraction, β is the difference in the FWHM of the peak between the sample and the standard SiO_2 used to calibrate the intrinsic width associated with the instruments, and λ is the wavelength of the X-ray. The calculated average grain size D_{hkl} is also listed in Table 1. It is clear from the table that the average crystallite size values are found to be in the range of 170–175 nm.

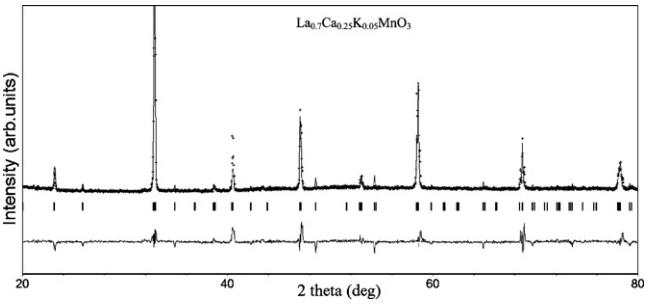

Fig. 2. Rietveld refinement of XRD pattern for $La_{0.7}Ca_{0.25}K_{0.05}MnO_3$. Crosses indicate the experimental data and the calculated data is the continuous line overlapping them. The lowest curve shows the difference between experimental and calculated patterns. The vertical bars indicate the expected reflection positions.

The temperature dependence of magnetization *M* (*T*) was measured under both the zero-field-cooling (ZFC) and the field-cooling (FC) modes at an applied field of 0.01 T in the temperature range 5–320 K. The ZFC and FC *M* (*T*) curves almost overlap in the whole studied temperature range and only the FC results are shown in Fig. 3. Very sharp paramagnetic (PM) to FM phase transitions are observed in the magnetization curves except for the Na-doped sample. The PM–FM transition in the Na-doped sample broadens obviously than the other samples. The broadened transition may be related to the existence of phase-separation phenomenon as discussed below. The transition temperature T_C (determined as the peak temperature of the d*M*/d*T* vs. *T* curve) are 217, 235, 253, and 237 K for the Li-, free-, Na-, and K-doped samples. The much smaller T_C values compared to earlier report may attribute to the oxygen deficiency formed in the high-temperature sintered progress [21]. The result shows that the Curie temperature T_C shifts to higher values with increasing $\langle r_A \rangle$ except for the K-doped sample, which agree well with the results report earlier [3,8,22]. According to the DE

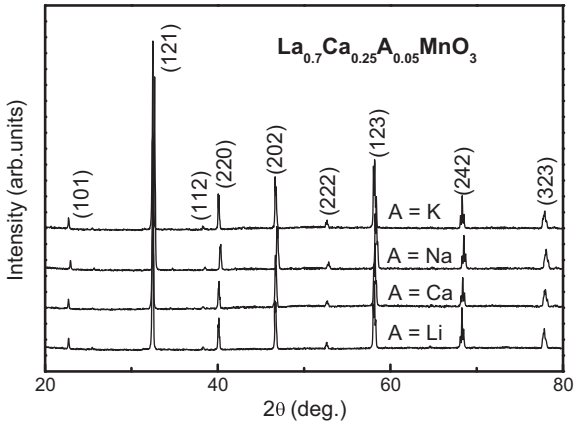

Fig. 1. Room-temperature X-ray diffraction patterns of $La_{0.7}Ca_{0.25}A_{0.05}MnO_3$ samples (A = Li, Ca, Na, and K).

Table 1
The A-site average cation radius $\langle r_A \rangle$, A-site-cation mismatch σ^2, average grain size D_{hkl}, and the refined structural parameters of $La_{0.7}Ca_{0.25}A_{0.05}MnO_3$ samples at room temperature.

Parameters	A = Li	A = Ca	A = Na	A = K
a (Å)	5.4614	5.4661	5.4643	5.4649
b (Å)	5.4746	5.4777	5.4786	5.4814
c (Å)	7.7295	7.7468	7.7370	7.7375
V (Å^3)	231.10	231.95	231.62	231.78
$d_{Mn-O(1)}$ (Å)	1.967	1.959	1.971	1.988
$d_{Mn-O(2)}$ (Å)	1.964	1.969	1.899	1.885
$\langle d_{Mn-Mn} \rangle$ (Å)	1.967	1.962	1.981	1.989
	1.966	1.961	1.953	1.951
$\theta_{Mn-O(1)-Mn}$ (°)	160.17	160.91	156.68	155.31
$\theta_{Mn-O(2)-Mn}$ (°)	159.32	160.25	166.33	169.26
$\langle \theta_{Mn-O-Mn} \rangle$ (°)	159.75	160.58	161.51	162.29
D_{hkl} (nm)	171.3	173.6	173.7	174.8
$\langle r_A \rangle$ (Å)	1.138	1.148	1.151	1.1675
σ^2 (Å^2)	0.0028	0.00034	0.00034	0.0065
R_p (%)	8.72	8.17	7.76	8.54

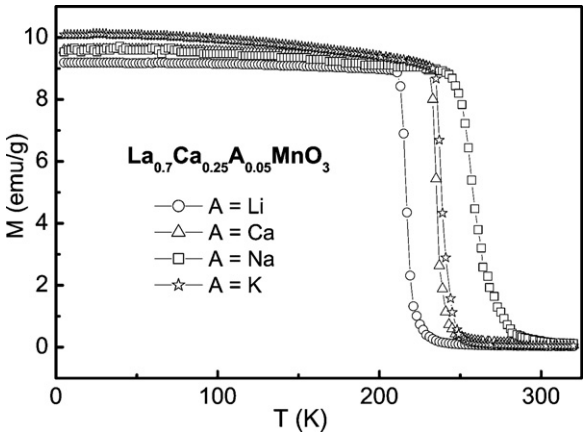

Fig. 3. Temperature dependence of FC magnetization of $La_{0.7}Ca_{0.25}A_{0.05}MnO_3$ manganites.

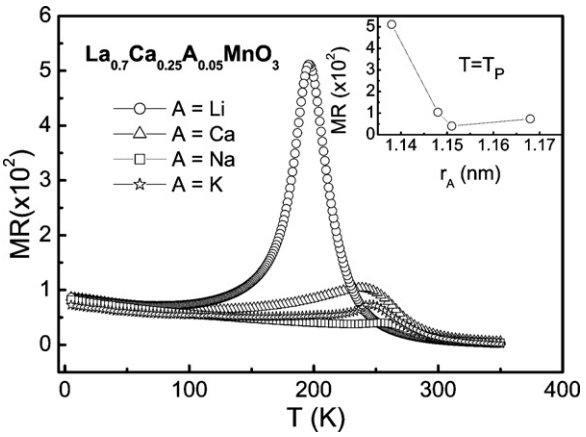

Fig. 5. The temperature dependence of magnetoresistance (MR) ratio of $La_{0.7}Ca_{0.25}A_{0.05}MnO_3$ at applied magnetic fields of 5 T. The inset shows the $\langle r_A \rangle$ dependence of MR at T_P.

interaction model, the overlap between Mn-3d and O-2p orbitals in perovskite manganites forms the electronically active band, which characterized by the one-electron bandwidth W. The Mn–O bond distance and the Mn–O–Mn bond angle are the two key parameters in controlling the variation of W. The decrease of the Mn–O bond distance and the increase of the Mn–O–Mn bond angle with increasing $\langle r_A \rangle$ may enhance the one-electron bandwidth in present studied samples, which result in the increase of T_C. With further increasing $\langle r_A \rangle$ for the K-doped sample, the A-site-cation mismatch effect prevails over the effect of the increasing $\langle r_A \rangle$ leading to the decrease of T_C.

To investigate the effect of mono-metal-doping effect at Ca sites on the electronic transport property of the samples, the temperature dependence of resistivity $\rho(T)$ was measured at zero applied magnetic field in the temperature range 5–350 K. The results are shown in Fig. 4. All the samples exhibit metallic transport behavior at low temperatures and undergo an obvious metal–insulator transition at a certain temperature T_P. The values of T_P are 189, 234, 254, and 243 K for the Li-, free-, Na-, and K-doped samples, respectively. T_P values of the free-, Na-, and K-doped samples are very close to their corresponding Curie temperature T_C, while for the Li-doped sample it is far below its T_C value (~28 K), associated with a pronounced increase in resistivity. The large difference between T_P and T_C of Li-doped sample may be due to the small grain size of the sample as shown in Table 1. The small grain size leads to the increase of charge carrier scattering at grain boundaries and poor connectivity between grains and then the increase of the resistivity.

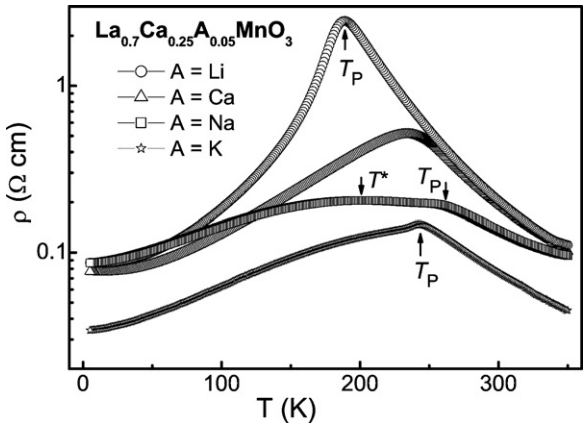

Fig. 4. Electrical resistivity vs. temperature of $La_{0.7}Ca_{0.25}A_{0.05}MnO_3$ (A = Li, Ca, Na and K) manganites.

Similar result is also observed in other $La_{0.67}Ca_{0.33}MnO_3$ samples prepared by both solid-state reaction and sol–gel methods [16,23]. Except for the transition at T_P, another small and very broader peak is observed at T^* (~201 K, as shown in Fig. 4) far below T_P in the $\rho(T)$ curve of the Na-doped sample. The observed two-peak behavior in $\rho(T)$ curve may be attributed to the difference in the magnetic order between the surface and core of the materials as discussed in the $La_{0.85}Sr_{0.15}MnO_3$ system [24]. The two magnetic order lead to the broader magnetic transition in the sample as aforementioned and the coexistence regions have different transport features.

The temperature dependence of resistivity of the studied samples was also measured under the action of applied magnetic field of 5 T. For all samples, $\rho(T)$ is markedly decreased under the applied field and shows a magnetoresistance (MR) effect as shown in Fig. 5. Here, MR is defined as $MR = [\rho(0) - \rho(5\ T)]/\rho(5\ T) \times 100\%$, where $\rho(0)$ is the resistivity at zero field and $\rho(5\ T)$ is the resistivity at an applied field of 5 T. Fig. 5 shows that MR of all samples exhibits an obvious peak around T_P originating from the suppression of intrinsic spin-dependent scattering within the grains. With decreasing temperature, MR increases slowly and monotonously stemming from the spin-dependent transfer of charge carriers through intergrain regions [25]. MR values at T_P against $\langle r_A \rangle$ for the four samples are plotted in the inset of Fig. 5. The Li-doped sample exhibits the largest MR value of 512% at its T_P among the studied samples. With increasing $\langle r_A \rangle$, MR at T_P decreases rapidly to 40.1% for the Na-doped sample. As $\langle r_A \rangle$ increases further, the role of A-site-cation disorder on MR becomes important resulting the increase of MR for the K-doped sample.

In order to further investigate the magneto-behavior in present studied samples, we carried out magnetization measurements vs. magnetic field up to 4.52 T at several temperatures. For each measurement, the sample was first heated to a certain temperature well above T_C, then, slowly cooled down to the settle temperature at zero magnetic fields. A typical result for the Li-doped sample is shown in Fig. 6. The obtained isothermal magnetization results allow us to determine the magnetic entropy changes ΔS_M of the studied samples. In general, the magnetic entropy of a material is associated with the magnetic degrees of freedom, which varies as the applied magnetic field changes the magnetic order of the material. From the classical thermodynamic theory based on Maxwell's thermodynamic relation, ΔS_M associated with a magnetic field variation from 0 to H_{max} can be induced by [26]

$$\Delta S_M(T,H) = S_M(T,H) - S_M(T,0) = \int_0^{H_{max}} \left(\frac{\partial M}{\partial T}\right)_H dH \quad (1)$$

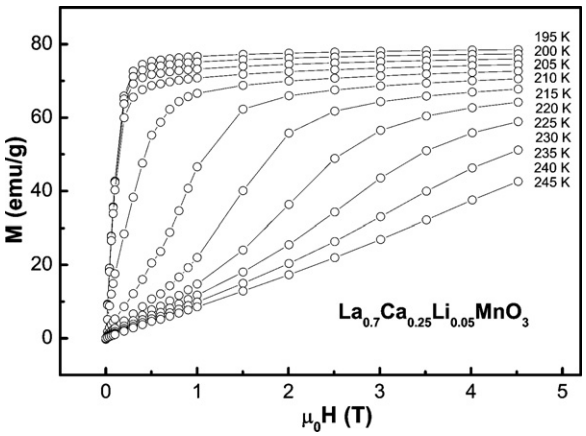

Fig. 6. Isothermal magnetization curves for $La_{0.7}Ca_{0.25}Li_{0.05}MnO_3$ polycrystalline sample measured at different temperatures between 195 and 245 K in the temperature interval of 5 K.

in the case of magnetization measurement at small discrete magnetic field and temperature intervals, $|\Delta S_M|$ can be approximated through the following equation:

$$\left|\Delta S_M\right| = \sum_i \frac{M_i - M_{i+1}}{T_{i+1} - T_i} \Delta H_i \quad (2)$$

in above expression, M_i and M_{i+1} are the experimental data of the magnetization under a magnetic field of H_i measured at T_i and T_{i+1}, respectively.

The calculated $|\Delta S_M|$ values as a function of temperature at $\Delta H = 0.5$, 1, 2, 3, 4 and 4.52 T for the Li-, free-, Na-, and K-doped samples are plotted in Fig. 7(a)–(d), respectively. As expected from Eq. (2), ΔS_M varies with temperature and reaches to their maximum at relative PM–FM transition temperature T_C, while ΔS_M distributes over a relative wide temperature range. The maximum magnetic entropy changes ΔS_{Mmax} obtained in the Li-, free-, Na-, and K-doped samples are 6.63, 7.03, 4.98, and 4.43 J/kg K, respectively, under a magnetic field of 2 T. One can see that the ΔS_{Mmax} values of our samples are much larger than that of similar compounds under the same field change of 2 T as reported earlier [9,27]. The results show that the perovskite manganites prepared using present sol–gel method could be potential good working materials for magnetic refrigeration in household refrigerators or air conditionings. Another interesting feature of present work is that the value of ΔS_{Mmax} has a contrary change trend with that of the A-site-cation mismatch σ^2. The K-doped sample with the largest σ^2 has the smallest ΔS_M values, whereas the free-doped sample has the largest ΔS_M values. In general, the large ΔS_M in perovskite manganites mainly originates from the considerable variation of M in the vicinity of the PM–FM transition temperature T_C. Moreover, the spin–lattice coupling in the magnetic ordering process also plays an important role on the large magnetic entropy changes in manganites [12]. The local lattice distortion increasing with A-site-disorder degree weakens the spin-lattice coupling and DE interaction in the Mn^{3+}–O–Mn^{4+} networks. It may be the reason of the small magnetic entropy changes for the samples with larger A-site-disorder (K- and Li-doped samples).

In the magnetic refrigeration technology, the most meaningful parameter characterizing the efficiency of a magnetocaloric material is the relative cooling power (RCP). The RCP value is always defined as [13]

$$\mathrm{RCP} = -\Delta S_M(T, H) \times \delta T_{FWHM}$$

here δT_{FWHM} stands the full-width at half maximum of $-\Delta S_M$ in the $-\Delta S_M$ vs. T curve. The calculated RCP values for all the samples at different magnetic fields are shown in Table 2. It is shown that the RCP values are also sensitive to the A-site-cation mismatch σ^2. The maximum RCP value is found to be 249 J/kg for a field change of 4.52 T for the free-doped sample $La_{0.7}Ca_{0.3}MnO_3$. In particular, large values of RCP are obtained to be 108.9, 106.1, 98.6, and 106.8 J/kg at a relative low field change of 2 T for the Li-, free-, Na-, and K-doped samples, respectively. The obtained RCP values are about 60% of pure Gd metal with a same field change of 2 T [28]. Although the values of RCP for present samples are smaller than that of conventional magnetic refrigerant materials, perovskite manganites

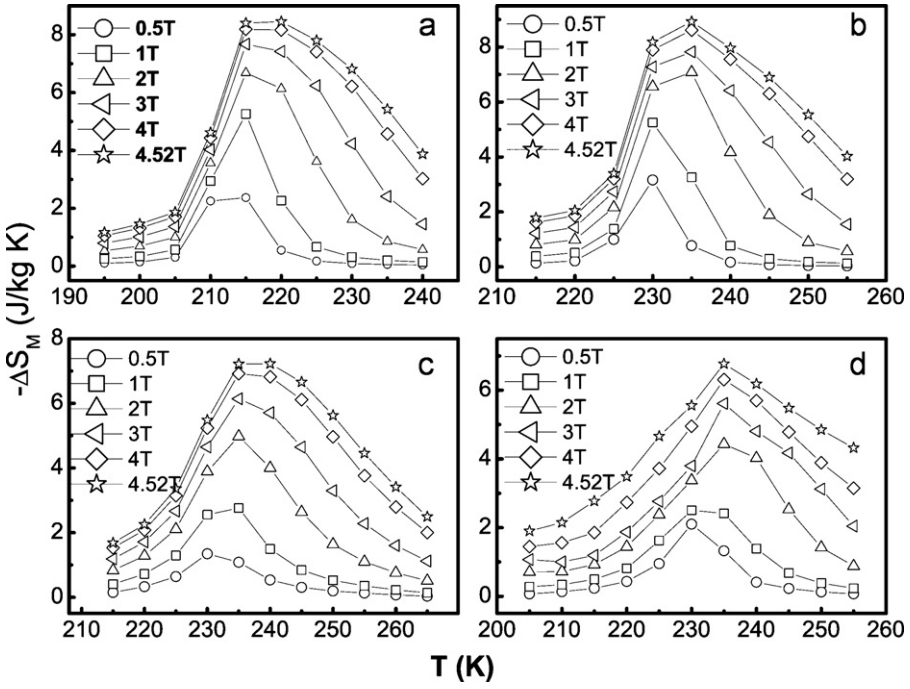

Fig. 7. Temperature dependence of magnetic entropy change $-\Delta S_M$ under $\Delta H = 0.5$, 1, 2, 3, 4 and 4.52 T for $La_{0.7}Ca_{0.25}A_{0.05}MnO_3$ samples with A = Li (a), Ca (b), Na (c) and K (d), respectively.

Table 2
The relative cooling power of $La_{0.7}Ca_{0.25}A_{0.05}MnO_3$ samples.

RCP (J/kg)	A = Li	A = Ca	A = Na	A = K
0.5 T	23.4	22.1	18.3	25.2
1 T	53.2	52.5	42.8	49.1
2 T	108.9	106.1	98.6	106.8
3 T	164.2	164.3	154.7	157.1
4 T	221.9	215.4	213.1	198.8
4.52 T	246.9	249.9	240.7	239.8

are inexpensive, good chemical stability, easier to fabricate, and tunable T_C by element doping, and therefore could be promising candidates for magnetic refrigeration.

4. Conclusion

The influence of disorder (the A-site average cation radius $\langle r_A \rangle$ and A-site-cation mismatch σ^2) on the structural, resistivity, magnetic, MR and magnetocaloric properties of mono-valence-metal-doped and free-doped $La_{0.7}Ca_{0.3}MnO_3$ polycrystalline samples has been investigated. All samples show an orthorhombic structure with *Pnma* space group at room temperature. The lattice parameters increase continuously as the dopant element changes from Li, Na to K. Sharp PM–FM and M–I phase transition are observed for all studied samples. The transition temperature of the Na-doped sample is the highest, whereas the Li-doped sample has the lowest one. In addition, the magnetic entropy change of the free-doped sample is the largest among the studied samples. The results can be explained well by the combined effect of the variation of the A-site average ionic radius $\langle r_A \rangle$ and A-site-cation mismatch σ^2.

Acknowledgments

This work was supported by the Nature Science Foundation of Anhui Province of China under Contract No. 090414184, the National Nature Science Foundation of China under Contract No. 10804111, and National Key Basic Research under contract No. 2007CB925002.

References

[1] A.M. Haghiri-Gosnet, J.P. Renard, J. Phys. D: Appl. Phys. 36 (2003) R127–R150.
[2] C. Zener, Phys. Rev. 82 (1951) 403–405.
[3] L.M. Rodriguez-Martinez, J.P. Attfield, Phys. Rev. B 54 (1996) 15622–15625.
[4] H.Y. Hwang, S.W. Cheong, P.G. Radaelli, M. Marezio, B. Batlogg, Phys. Rev. Lett. 75 (1995) 914–917.
[5] J. Fontcuberta, B. Martinez, A. Seffar, S. Pinol, J.L. GarciaMunoz, X. Obradors, Phys. Rev. Lett. 76 (1996) 1122–1125.
[6] A. Barnabe, A. Maignan, M. Hervieu, F. Damay, C. Martin, B. Raveau, Appl. Phys. Lett. 71 (1997) 3907–3909.
[7] L. Sheng, D.N. Sheng, C.S. Ting, Phys. Rev. B 59 (1999) 13550–13553.
[8] L.M. Rodriguez-Martinez, J.P. Attfield, Phys. Rev. B 58 (1998) 2426–2429.
[9] M. Bejar, E. Dhahri, E.K. Hlil, S. Heniti, J. Alloys Compd. 440 (2007) 36–42.
[10] N. Rama, M.S.R. Rao, V. Sankaranarayanan, P. Majewski, S. Gepraegs, M. Opel, R. Gross, Phys. Rev. B 70 (2004).
[11] X. Bohigas, J. Tejada, M.L. Marinez-Sarrion, S. Tripp, R. Black, J. Magn. Magn. Mater. 208 (2000) 85–92.
[12] Z.B. Guo, Y.W. Du, J.S. Zhu, H. Huang, W.P. Ding, D. Feng, Phys. Rev. Lett. 78 (1997) 1142–1145.
[13] M.H. Phan, S.C. Yu, J. Magn. Magn. Mater. 308 (2007) 325–340.
[14] W.C.R. Koubaa, M. Koubaa, A. Cheikhrouhou, J. Mater. Sci. 44 (2009) 1780–1786.
[15] Q. Ji, B. Lv, P.F. Wang, H.L. Cai, X.S. Wu, G.H. Liu, G.S. Luo, J. Appl. Phys. 105 (2009) 07D713.
[16] M. Koubaa, W. Cheikhrouhou-Koubaa, A. Cheikhrouhou, A.M. Haghiri-Gosnet, Physica B 403 (2008) 2477–2483.
[17] G.Q. Zhang, C.X. Pan, Q.X. Zhou, Solid State Commun. 141 (2007) 471–473.
[18] T. Shimura, T. Hayashi, Y. Inaguma, M. Itoh, J. Solid State Chem. 124 (1996) 250–263.
[19] R.D. Shannon, Acta Crystallogr. Sect. A 32 (1976) 751–767.
[20] M.I. Mendelso, J. Am. Ceram. Soc. 52 (1969) 443–446.
[21] R. Dhahri, F. Halouni, J. Alloys Compd. 385 (2004) 48–52.
[22] T. Terai, T. Kakeshita, T. Fukuda, T. Saburi, N. Takamoto, K. Kindo, M. Honda, Phys. Rev. B 58 (1998) 14908–14912.
[23] G. Venkataiah, D.C. Krishna, M. Vithal, S.S. Rao, S.V. Bhat, V. Prasad, S.V. Subramanyam, P.V. Reddy, Physica B 357 (2005) 370–379.
[24] N. Zhang, W.P. Ding, W. Zhong, D.Y. Xing, Y.W. Du, Phys. Rev. B 56 (1997) 8138–8142.
[25] B.C. Zhao, W.H. Song, Y.Q. Ma, R.L. Zhang, J. Yang, Z.G. Sheng, W.J. Lu, J.M. Dai, Y.P. Sun, Phys. Status Solidi B: Basic Solid State Phys. 242 (2005) 1719–1727.
[26] K.A. Gschneidner, V.K. Pecharsky, Annu. Rev. Mater. Sci. 30 (2000) 387–429.
[27] M. Bejar, R. Dhahri, E. Dhahri, M. Balli, E.K. Hlil, J. Alloys Compd. 442 (2007) 136–138.
[28] J.W. Byeon, C.S. Kim, S.I. Kwun, Phys. Status Solidi B: Basic Res. 241 (2004) 1756–1760.